CrossMark

ORIGINAL PAPER

Fischer–Tropsch Synthesis Over Zr-Promoted Co/γ-Al$_2$O$_3$ Catalysts

Javier Barrientos[1] · Victoria Garcilaso[2] · Baldassarre Venezia[1] · Atte Aho[3] ·
José Antonio Odriozola[2] · Magali Boutonnet[1] · Sven Järås[1]

Abstract Two Zr-modified alumina supports were synthetized containing the same amount of Zr but a different distribution of this modifier over the alumina surface. These supports, together with the unmodified alumina carrier, were used to prepare three cobalt-based catalysts which were characterized and tested under relevant Fischer–Tropsch conditions. The three catalysts presented very similar porosity and cobalt dispersion. The addition of Zr nor its distribution enhanced the catalyst reducibility. The catalyst activity was superior when using a carrier consisting of large ZrO$_2$ islands over the alumina surface. The use of a carrier with a homogeneous Zr distribution had however, a detrimental effect. Moreover, a faster initial deactivation rate was observed for the Zr-promoted catalysts, fact that may explain this contradictory effect of Zr on activity. Finally, the addition of Zr showed a clear enhancement of the selectivity to long chain hydrocarbons and ethylene, especially when Zr was well dispersed.

Keywords Fischer–Tropsch synthesis · Co/Al$_2$O$_3$ · Cobalt · Zr · Activity

✉ Javier Barrientos
  javbar@kth.se

1 KTH (Royal Institute of Technology), Chemical Science and Engineering, Chemical Technology, Teknikringen 42, Plant 6, 100 44 Stockholm, Sweden

2 Química de Superficies y Catálisis, Instituto de Ciencia de los Materiales (US-CSIC), Av. Américo Vespucio no. 49, 41092 Sevilla, Spain

3 Johan Gadolin Process Chemistry Centre, Åbo Akademi University, Biskopsgatan 8, 20500 Åbo/turku, Finland

1 Introduction

The Fischer–Tropsch synthesis (FTS), i.e. the conversion of CO and H$_2$ into hydrocarbons, is a widely known industrial catalytic process and key step in the transformation of carbonaceous sources (e.g. coal, natural gas and biomass) into liquid fuels [1, 2]. Supported cobalt catalysts have received great attention in FTS due to their high activity and selectivity to long chain hydrocarbons [3, 4]. Among different supports, Al$_2$O$_3$ is often used due to its high attrition resistance and its suitability in slurry bubble column reactors [5, 6]. Unfortunately, Co/Al$_2$O$_3$ catalysts present a hard reducibility due to the strong interaction between alumina and small cobalt oxide crystallites [7, 8]. A high degree of reduction is desired in order to maximize the Co^0 site density and so, the activity of the catalyst.

This problem can be overcome, to a certain extent, by using promoters. One solution is to promote Co/Al$_2$O$_3$ catalysts with small amounts of noble metals (e.g. Pt, Re and Ru) [9–11]. This promoting effect is generally explained by a H$_2$ spillover mechanism, i.e. dissociative chemisorption of H$_2$ and migration of H adatoms from the noble metal surface to the cobalt oxide surface [12–14]. Another solution is to modify the alumina support with an oxide promoter that offers a better cobalt-support interaction. Several studies have used promoters such as Zr [15–17], La [18], Mg [19], Mn [20], Ti [21] or Ce oxides [22] and most of them were reported to improve the catalyst activity.

The effect of Zr on the performance of Co/Al$_2$O$_3$ catalysts has already been investigated by various researchers [15–17, 20, 23–25]. Yet, there is no consensus in what concerns its promoting effect. In the work of Rohr et al. [15] they evaluated the performance of Co/Al$_2$O$_3$ catalysts with Zr loadings varying from 0 to 10 wt%. They found that Zr has no influence on the reducibility but

Springer

enhances the turnover frequency (TOF) and the selectivity to long chain hydrocarbons. Steady state isotopic transient kinetic analyses (SSITKA) revealed that the enhancement of the TOF was due to a change in the surface coverage of active intermediates and not to an increase of the intrinsic TOF, i.e. the TOF divided by the number of active surface intermediates. A similar study was later performed by Jongsomjit et al. [16] using catalysts containing between 0 and 11 wt% of ZrO_2. Nevertheless, they found that Zr enhances both the reducibility and the TOF. The authors also performed SSITKA experiments and obtained results comparable to those found by Rohr et al. [15]. However, they claimed that the number of active intermediates is probably a better measurement of cobalt active sites than that obtained from standard H_2 chemisorption methods [26], and thus, suggested that Zr only enhances the reducibility but not the TOF.

Other researchers [23] have showed that modification with 10 wt% of ZrO_2 can lead to smaller cobalt particles inside the pores and, as a result, limit the catalyst reducibility. Ma et al. [24] found that addition of 1–5 wt% Zr enhances the reducibility of narrow pore Co/γ-Al_2O_3 catalysts (mean pore size: 4–5 nm) but it does not have any influence on wide pore Co/γ-Al_2O_3 (mean pore size: 7–8 nm). The reported TOF values were similar for all the catalysts. It may be worth mentioning that they also found that Zr increases the deactivation rate. Moreover, Shimura et al. [20] showed that the addition of 1 wt% Zr to Co/θ-Al_2O_3 catalysts has no impact on the reducibility nor the activity of the catalyst.

It may be noted that some discrepancies exist as well between studies promoting Co/SiO_2 catalysts with ZrO_2. Besides some studies [27], Zr has often been reported to increase the TOF [28–33]. However, some researchers [28–30] found that ZrO_2 enhances the reducibility while others [31] claim that it does not have any influence. Finally, Hong et al. [32] found that Zr favors the reducibility in narrow pore Co/SiO_2 catalysts (mean pore size: 2–3 nm) but not in wide pore catalysts (mean pore size: 7–8 nm).

The present work aims to further investigate this effect of Zr on the reducibility and catalytic performance of Co/γ-Al_2O_3 catalysts at industrially relevant FTS conditions. The effect of the Zr distribution over the alumina surface was also evaluated in order to study the effect of this promoter from a different perspective. For that purpose, two Zr-modified alumina carriers were synthetized using different preparation methods. These two supports and the unmodified alumina carrier were further used to synthetize cobalt FTS catalysts with similar morphology and cobalt dispersion but a different cobalt-support interaction.

2 Experimental

2.1 Catalyst Preparation

A ZrO_2-modified alumina carrier was prepared using a conventional precipitation technique. For that purpose, a salt of $ZrO(NO_3)_2 \cdot xH_2O$ (Sigma Aldrich, 99%) was dissolved in EtOH (Merck, Abs Analytical grade). The alumina carrier was then added to the liquid solution and stirred for 30 min. Afterwards, the mixture was treated with an NH_3 aqueous solution 1:1 v/v H_2O /NH_3 (30% Panreac) under stirring for 30 min. Finally, the solid was filtered, dried at 100 °C for 24 h, and calcined at 500 °C (heating rate: 10 °C/min) for 4 h in air. This support was named "ZrAl P".

Another ZrO_2-modified support, using the same γ-Al_2O_3 carrier, was prepared by the microemulsion technique. For that purpose, an aqueous solution $ZrO(NO_3)_2 \cdot xH_2O$ (Sigma Aldrich, 99%) was dissolved in Milli-Q™ water. Then, this aqueous solution was used to prepare a water-in-oil microemulsion (ME) system. A water-in-oil ME is an optically transparent and thermodynamically stable solution which consists of aqueous nanodroplets stabilized by a layer of surfactant molecules [34]. Metal salts dissolved in the core of these nanodroplets can then be precipitated in form of particles in a nano-sized range [34]. The composition of the ME system is given in Table 1. Once the ME was achieved, the alumina carrier was added. Then, NH_3 was added to the mixture until achieving a pH 11. The mixture was kept under vigorous stirring for a period of 24 h. The solids were then separated by centrifugation and cleaned with a 1:1 v/v solution of EtOH and $CHCl_3$. The centrifugation-rinsing procedure was repeated a total of 3 times. Finally, the sample was dried at 70 °C for 24 h and calcined at 500 °C (heating rate: 10 °C/min) for 4 h in air. This support was named "ZrAl ME".

A third support was prepared by calcining the unmodified alumina carrier at 500 °C (heating rate: 10 °C/min) for 4 h in air. This support was named "Al". The three supports were prepared using the commercial γ-Al_2O_3 carrier Spheres Sasol® 1.8/210 crushed into a fine powder (mesh: 53–90 μm).

Table 1 Composition of the ME system

Phase	Compounds	Composition (wt%)
Oil (continuous phase)	Isooctane	71
Surfactant	Synperonic™ 91/5 (Polyoxyethylene C9-C11 alcohol)	22.9
Water (nanodroplets)	Milli-Q™ water	5.53
	$ZrO(NO_3)_2$	0.57

The incipient wetness impregnation technique was used to deposit 12 wt% of cobalt on the prepared supports. The supports were impregnated with an aqueous solution of $Co(NO_3)_2 \cdot 6H_2O$ (ACS reagent, ≥98% Sigma Aldrich). Due to the large volume of water required to dissolve the salt, the aqueous solution was deposited batch wise, drying the samples at 100 °C for 2 h after each deposition. A total of 3 batches were needed for complete deposition of the aqueous solution. Finally, the impregnated powders were dried at 120 °C for 3 h (heating rate: 5 °C/min) and calcined at 300 °C (heating rate: 1 °C/min) for 16 h in air. Thus, a total of 3 catalysts were prepared and named according to the names of the supports: "CoAl", "CoZrAl P" and "CoZrAl ME".

2.2 Catalyst Characterization

2.2.1 N_2 Adsorption–Desorption

N_2 adsorption–desorption measurements were performed in a Micromeritics ASAP 2000/2010 unit in order to estimate the Brunauer–Emmett–Teller (BET) surface area and porosity of the catalysts and supports. The samples were evacuated and dried overnight at 250 °C prior to analysis. The BET surface area was estimated by adsorption at liquid nitrogen temperature at relative pressures between 0.06 and 0.2. The pore volume was estimated from a single point of adsorption at a relative pressure of 0.992. The mean pore diameter was estimated from the pore volume and the surface area assuming cylindrical pores. The pore size range was calculated with the Barrett–Joyner–Halenda (BJH) method using the desorption isotherm.

2.2.2 Inductively Coupled Plasma Mass Spectrometry

The Zr-modified supports were analyzed by inductively coupled plasma mass spectrometry (ICP-MS) in order to determine the Zr loading. The analyses were performed by ALS Scandinavia.

2.2.3 Transmission and Scanning Electron Microscopy

Transmission electron microscopy (TEM) images presented on this paper were recorder on a PHILIPS CM-200 instrument with spot size of 15 nm and resolution of 2.8 Å. The samples were supported on a holey carbon-coated copper grid using an ethanoic suspension. The Digital Micrograph™ software from Gatan Inc. was used for treatment of the images.

The surface of the supports was observed with a Hitachi® S-4800 SEM-FEG microscope (SEM) provided with secondary and retro-dispersed electron detector. An energy-dispersive X-ray spectroscopy (EDS) mapping was carried out by means of a Bruker X Flash Detector 4010, with resolution of 133 eV. Compositional mapping measurements were carried out using an accelerating voltage of 15 KV in order to evaluate the distribution of Zr and Al over the support surface.

2.2.4 Acidity Measurements

Ammonia temperature-programmed desorption (NH_3-TPD) analyses were performed in order to study the acidity of the supports. NH_3-TPD measurements of ca. 0.2 g of the support samples were performed in a Micromeritics AutoChem 2910 unit equipped with a thermal conductivity detector (TCD). Prior to analysis, the samples were pretreated at 500 °C (heating rate: 10 °C/min) for 1 h in flowing He (30 NmL/min). Afterwards, the samples were cooled down to room temperature and exposed to a flow 5% NH_3 in He (30 NmL/min) for 1 h. Then, these were purged with He flow (100 NmL/min) at 100 °C (heating rate: 10 °C) for 1 h in order to remove physically adsorbed NH_3. Finally, the samples were heated up in He (30 NmL/min) from room temperature to 500 °C (heating rate: 10 °C/min) while monitoring the difference in thermal conductivity between the inlet and the outlet gas.

The Brønsted and Lewis acidity of the catalysts was measured by infrared spectroscopy (ATI Mattson FTIR) using pyridine as a probe molecule. A thin (15–30 mg) self-supported wafer of the catalyst was pressed and then placed into the FTIR-cell. The cell was evacuated and the temperature was raised to 450 °C and kept for 1 h. Thereafter, the temperature was decreased to 100 °C and the background spectra of the sample were recorded. Pyridine was adsorbed on the sample for 30 min at 100 °C followed by desorption at 150, 250 and 350 °C for 1 h and the spectra of the sample were recorded in between every temperature ramp. The scanning was performed under vacuum at 100 °C. Spectral bands at 1545 cm^{-1} and at 1450 cm^{-1} were used to identify Brønsted and Lewis acid sites, respectively. The quantitative amount of the acid sites was calculated with the constants of Emeis [35].

2.2.5 Temperature-Programmed Reduction

The reducibility of the catalysts was studied by hydrogen temperature-programmed reduction (TPR) analyses in the same Micromeritics AutoChem 2910 unit. The analyses were performed by heating up the calcined samples up to 1000 °C (ramp: 10 °C/min) in a 5% H_2 in Ar flow while monitoring the difference in thermal conductivity between the inlet and the outlet gas. The TCD signal was calibrated by complete reduction of a reference Ag_2O powder in order to calculate the consumption of H_2.

The degree of reduction (DOR, %) was estimated by TPR after in situ reduction of the calcined catalysts at 350 °C (heating rate: 1 °C/min) for 16 h in pure H_2 flow. After reduction, the samples were flushed with inert gas for 30 min at 350 °C. Afterwards, the abovementioned TPR procedure was performed in order to estimate the amount of H_2 consumed when reducing the remaining cobalt oxides. The DOR was calculated assuming that the remaining cobalt oxides were in form of Co^{2+}.

2.2.6 H_2 and CO Chemisorption

Static chemisorption measurements were performed on the fresh catalysts using both H_2 and CO in order to estimate the cobalt dispersion (D, %) and the mean cobalt crystallite size [$(dCo^0)_H$, nm]. All the analyses were performed in a Micromeritics ASAP2020C unit after evacuation at 40 °C for 1 h and in situ reduction at 350 °C (heating rate: 1 °C/min) for 16 h in pure H_2 flow. After reduction, the samples were evacuated at 330 °C for 1 h and for 30 min at 100 °C prior to analysis. The method consists in obtaining an adsorption isotherm at 35 °C between 15 and 500 mmHg. The H_2 and CO uptakes were estimated by extrapolating the straight-line portion of the isotherm to zero pressure. After this analysis, the often called "reversible" and "irreversible" uptakes [26] were estimated by evacuating the samples at 10 µmHg for 1 h and repeating this method to obtain a second adsorption isotherm. The reversible uptake was determined by extrapolating to zero pressure this second isotherm. The irreversible uptake was calculated by taking the difference between the total and the reversible uptake. The metal dispersion was calculated from the total H_2 uptake assuming that the H:Co adsorption stoichiometry is 1:1 [26]. The $d(Co^0)_H$ was estimated assuming spherical particles according to the following equation [36]:

$$d\left(Co^0\right)_H = \frac{0.96}{D} \times DOR$$

2.2.7 X-ray Diffraction

X-ray diffraction (XRD) was performed on the calcined catalysts using a Siemens D5000 diffractometer with Cu-Kα radiation ($2\theta = 10°–90°$, step size $= 0.02°$) equipped with a Ni filter. The Co_3O_4 crystallite diameter [$d(Co_3O_4)_{XRD}$, nm] was estimated by using the Scherrer equation and assuming spherical crystallites and applying a correction factor of 4/3 [37, 38]. The cobalt crystallite size [$(dCo^0)_{XRD}$, nm] was estimated from that of Co_3O_4 according to the relative molar volumes of Co^0 and Co_3O_4 using the following formula [7]:

$$d(Co^0)_{XRD} = 0.75 \times d(Co_3O_4)_{XRD}$$

2.3 Catalytic Testing

The catalytic tests were performed in a down-flow stainless steel fixed bed reactor (i.d. 9 mm). The reactor was heated by means of an electric oven and the temperature was regulated by cascade control with one sliding thermocouple inside a thermowell placed inside the reactor and another thermocouple placed in the oven. All the tests were performed with approximately 1.5 g of dried catalyst samples diluted with ca. 10 g of SiC (mean particle size: 75 µm). This high catalyst dilution, together with an aluminum jacket placed between the reactor and the oven, allowed for an even temperature profile (210 ± 2 °C) along the catalyst bed. A catalyst particle size in the range of 53–90 µm was used in order to suppress the influence of mass transfer on the catalyst performance [3, 8, 39, 40].

The samples were in situ reduced at 350 °C (heating rate $= 1$ °C/min) for 16 h in pure H_2 flow [gas hourly space velocity $= 7.5$ NL/(h·$g_{catalyst}$)]. Afterwards, the reactor was cooled down to 180 °C and pressurized to 20 bars with He flow. Then the He flow was replaced by syngas (containing 3% N_2 as internal standard) and the temperature was increased to 195 °C (heating rate $= 0.5$ °C/min) and subsequently to 210 °C (heating rate $= 0.2$ °C/min). The tests were conducted at 210 °C, 20 bar and using a $H_2/CO = 2.1$.

The testing procedure consisted of four periods. In the first period (Period I) the catalysts were exposed to a GHSV of 10 NL/(h $g_{catalyst}$) for approximately 24 h. This first period served for determination of the catalyst initial activity and Site Time Yield (STY). In the second and third periods (Periods II and III) the GHSV was adjusted in order to expose the catalysts to 30 and 40% CO conversion, respectively. Each period had a duration of approximately 1 day. Since the water partial pressure (and so, the CO conversion) has an effect on the FT product distribution [8, 41–43], these two periods served for a proper comparison of the selectivity of the catalysts. In the last period (Period IV), the GHSV was adjusted again to operate at ca. 50% CO conversion. These conditions were maintained for 3 days in order to compare the deactivation rate of the catalysts.

The liquid hydrocarbons, waxes and water leaving the reactor were condensed in two consecutive traps at 140 °C and room temperature, respectively. The gases leaving the traps were depressurized and analyzed online with a gas chromatograph equipped with a TCD and a flame ionization detector (FID). H_2, N_2, CO, CH_4 and CO_2 were separated by a Carbosieve II packed column and analyzed on the TCD. C_1-C_6 products were separated by an alumina-plot column and quantified on the FID. The selectivity to C5+ products (S_{C5+}) was used to represent the selectivity to long chain hydrocarbons. The S C5+ was calculated as follows:

$$S_{C5+} = 100 - \left(S_{C1} + S_{C2} + S_{C3} + S_{C4} + S_{CO_2} \right)$$

3 Results and Discussion

3.1 Characterization of Supports and Catalysts

3.1.1 Surface Area and Porosity Measurements

The BET surface area, pore volume and average pore diameter as estimated by N_2 adsorption–desorption

Table 2 Physical properties of supports and catalysts after calcination

Sample	BET surface area (m^2/g)	Pore volume (mL/g)[a]	Mean pore diameter (nm)[b]	BJH mesopore volume (mL/g)[c]
Supports				
Al	202	0.51	10.1	0.40
ZrAl P	215	0.52	9.7	0.45
ZrAl ME	241	0.51	8.5	0.46
Catalysts				
CoAl	164	0.39	9.5	0.32
CoZrAl P	176	0.37	8.4	0.32
CoZrAl ME	189	0.38	8.0	0.33

[a] Total pore volume as estimated by a single point of adsorption at a relative pressure of 0.992

[b] Mean pore diameter calculated according to: $4 \cdot$ Pore volume/BET surface area

[c] Mesopore volume (volume of pores in the range of 1–50 nm) as estimated by using the BJH method

measurements are presented in Table 2. All the samples are characterized by a relatively high surface area and pore volume. It can be observed that the addition of ZrO_2 increased the BET surface area, especially for the carrier prepared by ME. This enhancement may be due to added surface crystalline defects or by an enhancement of the thermal resistance of the carrier during calcination. As can be deduced, the mesopore volume (pores in the range of 1–50 nm) constitutes between 80 and 90% of the total pore volume. Thus, the materials present mainly mesopores and possibly, in a minor extent, macropores.

The mesopore size distribution of both supports and catalysts is presented in Fig. 1. As can be observed, all the samples present a very similar pore size distribution. The majority of the pores have a diameter in the range of 5–10 nm. Moreover, the volume of these pores decreased after addition of cobalt, indicating that the metal particles were effectively deposited inside the carrier's mesoporous structure.

3.1.2 Physicochemical Properties of the Supports

The surface of the Zr-modified carriers was analyzed with SEM in order to study the distribution of ZrO_2 over the alumina carrier. Representative images of these two supports are presented in Fig. 2. The SEM images reveal that Zr is heterogeneously distributed on the ZrAl P support, forming large islands rich in ZrO_2 and poor in Al_2O_3. Contrariwise, the support prepared by ME shows a more homogeneous distribution. Further ICP-MS analyses of these two samples confirmed that both carriers contained 10 wt% of Zr. These images demonstrate how the ME technique can be successfully applied to homogenously disperse oxide promoters over a mesoporous support.
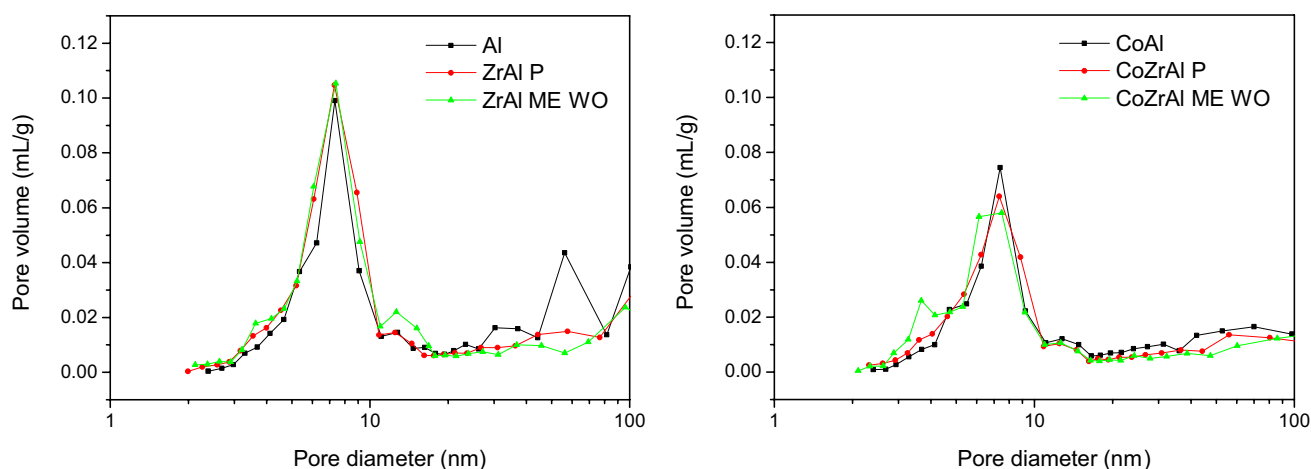

Fig. 1 BJH pore size distribution of supports (*left*) and catalysts (*right*)
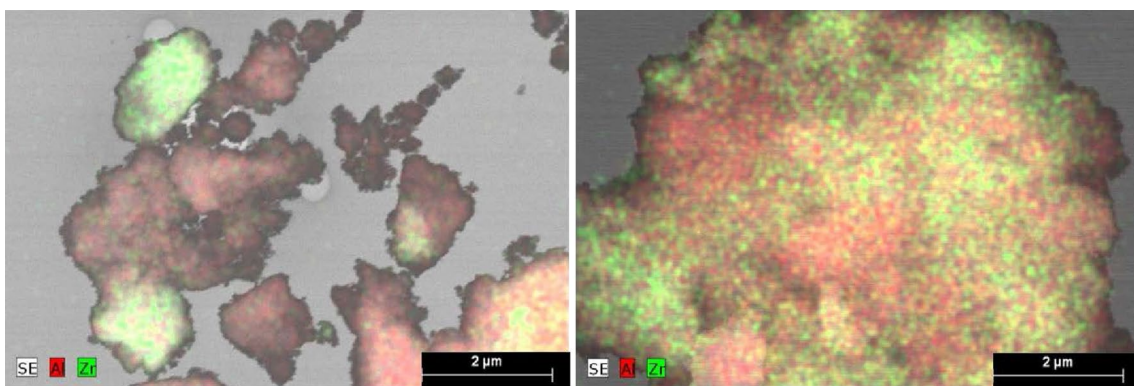
Fig. 2 Representative SEM images of the ZrAl P (*left*) and ZrAl ME (*right*) support. The colors *red* and *green* indicate the presence of Al and Zr, respectively
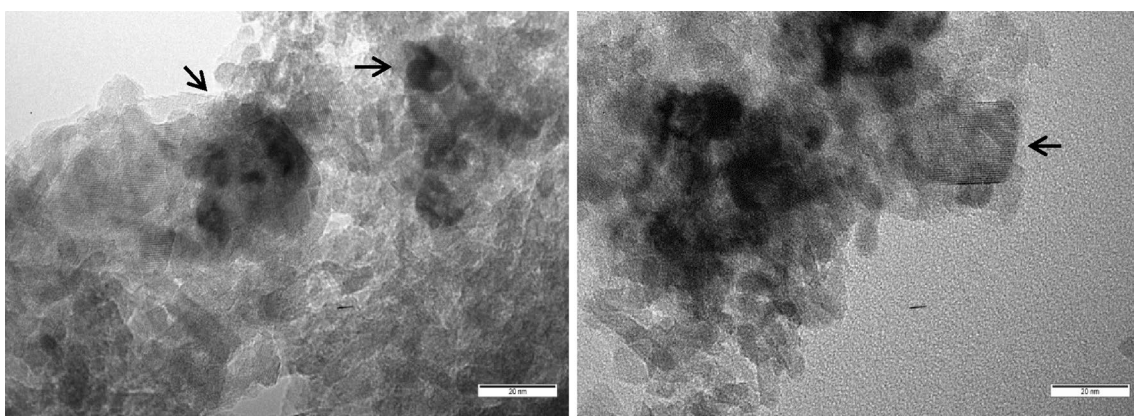

Fig. 3 Representative TEM images of: ZrAl P sample (*left*) and ZrAl ME sample (*right*). The *arrows* have been inserted to facilitate the identification of large crystallites

In Fig. 3 two representative TEM images of the ZrAl P and ZrAl ME samples are shown. As can be observed the supports presents high concentration of crystalline zones. The average interplanar spacing of crystals found in ZrAl P and ZrAl ME were respectively 4.62 and 4.68 Å which correspond to {111} γ-Al_2O_3 [44]. In agreement with Rozita et al. [45], the γ-Al_2O_3 morphology corresponds to facetted and elongated crystals forming agglomerates. In that review, they also concluded that the cubeoctahedral morphology, also observed in our samples, is often dominant in γ-Al_2O_3 carriers probably due to a preferential growth of these {111} facets. In the case of the Al support such abundancy of these crystalline zones was not observed; fact that suggests that the incorporation of ZrO_2 increases the support crystallinity.

The NH_3-TPD profiles are presented in Fig. 4. The profiles suggest the existence of two main peaks which may be ascribed to two types of acid sites with different strength. The total acidity of the supports is similar. However, the results indicate that the addition of Zr increases the density
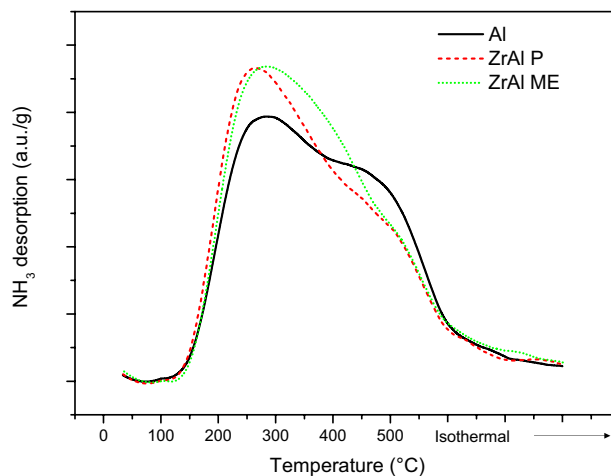

Fig. 4 NH_3 temperature-programmed desorption profiles for the Al, ZrAl P and ZrAl ME supports

Table 3 Distribution of Lewis acid sites in the supports as determined by FTIR spectroscopy of adsorbed pyridine

| Sample	Lewis acid sites (μmol/g)		
	150 °C	250 °C	350 °C
Al	116	54	15
ZrAl P	101	36	10
ZrAl ME	130	45	4

of weak acid sites (desorbing below 400 °C) and decreases the density of strong sites (desorbing above 400 °C). The profiles also suggest that the acidity of the ZrAl ME support is slightly higher than that of the ZrAl P.

The acid strength distribution of the supports, as obtained by FTIR spectroscopy of adsorbed pyridine, is listed in Table 3. The distribution of acid sites is fairly similar for all samples. No Brønsted acidity could be observed for any of the supports. The amount of Lewis acid sites of lower strength is slightly higher in the ZrAl ME support than in the ZrAl P, in line with the results obtained from NH$_3$-TPD.

Recent investigations have found that the support Lewis acidity plays an important role in cobalt-catalyzed FTS [46, 47]. Prieto et al. [46] found that the TOF and the selectivity to long chain hydrocarbons increases with increasing acidity of the oxide support. However, excessive acidity leads to a partial coverage of the cobalt particles by partially reduced oxide support species. This interplay between increasing the TOF and reducing the number of cobalt active sites results in a volcano dependence of the overall reaction rate with the carrier acid-base character. According to Johnson and Bell [47], this promoting effect of Lewis acid sites may be ascribed to their interaction with the O atom of adsorbed CO, which facilitates CO adsorption and dissociation. Unfortunately, the addition of Zr nor its distribution appear to enhance significantly the surface acidity of alumina. In this sense, no important changes in catalyst activity and selectivity should be expected.

3.1.3 Physicochemical Properties of the Catalysts

The temperature-programmed reduction (TPR) profiles of the three catalysts are presented in Fig. 5. These profiles reveal the existence of various peaks. The first peak, situated at a temperature around 300 °C, is ascribed to the reduction of Co^{3+} to Co^{2+} (i.e. Co$_3$O$_4$ to CoO) [8, 12, 14, 48]. The second peak, situated at ca. 400 °C, corresponds to the reduction of big CoO crystallites to metallic cobalt. The broad H$_2$ consumption area occurring above 600 °C is ascribed to the reduction of small CoO crystallites and cobalt-aluminate species [8, 12, 23, 49].
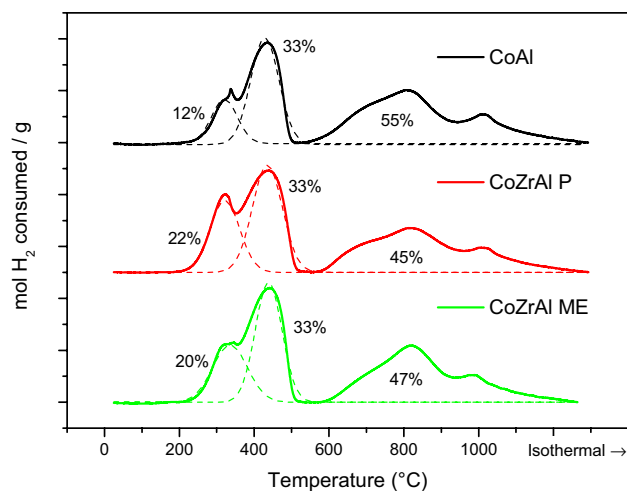
Fig. 5 Temperature-programmed reduction profiles of the three catalysts in 5% H$_2$ in Ar flow

Two main conclusions can be derived from these TPR profiles. Firstly, the amount of Co$_3$O$_4$ in the catalysts is different. The results suggest that the addition of Zr increases the amount of Co^{3+} after calcination. This could be associated to a lower formation of CoAl$_2$O$_4$. Nevertheless, this does not necessarily imply that Zr improves the catalyst reducibility since cobalt aluminates can form during reduction. Secondly, the addition of Zr does not shift the reduction peaks to lower temperatures. This second observation suggests, in contrast, that Zr does not improve the reducibility of the catalyst. For instance the use of Pt, which is widely accepted to improve the reducibility, moves the peaks approximately 50–100 °C to lower temperatures [12, 14, 50].

The estimated degrees of reduction (DOR) after 16 h at 350 °C in pure H$_2$ flow are presented in Table 4. The DOR's are low (around 40%) and similar for the three catalysts. These results were expectable since the TPR profiles indicate that most of the Co^{2+} reduces at a temperature above 600 °C. These small differences in the DOR number may be ascribed to the partial reduction of cobalt species reducing slightly above 600 °C. Indeed, the TPR profiles present slight changes in the region between 600 and 700 °C, which may be in line with the observed DOR's. Nevertheless, it cannot be discarded that such small differences are simply a result of instrument and procedure errors.

In conclusion, our results suggest that Zr has no or almost no effect on the catalyst reducibility. The observed differences in reducibility are rather small and it is not clear whether these can be assigned to a Zr effect or to slight differences in Co particle size distribution. In any case, this possible improving effect of Zr appears to be very small and not comparable to that of noble metal promoters. These results may be somewhat surprising since it has been found

Table 4 Catalyst physicochemical properties

Catalyst	DOR (%)[a]	d(Co$_3$O$_4$)$_{XRD}$ (nm)[b]	d(Co^0)$_{XRD}$ (nm)[c]
CoAl	42	13	10
CoZrAl P	44	15	11
CoZrAl ME	40	14	10

[a]Degree of reduction after 16 h at 350 °C in H$_2$ flow as estimated by temperature-programmed reduction

[b]Mean Co$_3$O$_4$ particle size as estimated by X-ray diffraction using the isolated peak situated between 58° and 62°

[c]Mean Co particle size as estimated from the Co$_3$O$_4$ mean particle size

that Co/ZrO$_2$ catalysts present better reducibility than Co/Al$_2$O$_3$ catalysts [51]. A possible explanation to these results is that the surface of these Zr-modified carriers was not completely covered by ZrO$_2$, as observed in the SEM images. The presence of superficial alumina may still lead to the formation of hardly reducible cobalt-support compounds. Therefore, we suggest that Zr may only improve

the reducibility when the support is practically or totally coated with ZrO$_2$ and thus, the catalyst behaves nearly as a Co/ZrO$_2$ catalyst. This explanation may also explain the slightly higher reducibility of the CoZrAl P catalyst whose surface presented large islands rich in Zr.

The X-ray diffractograms of the supports and the catalysts are presented in Fig. 6. As can be observed, by comparing the supports, a ZrO$_2$ peak appears at ca. 32° when ZrO$_2$ is added to the alumina carrier. The small size of this peak suggests that ZrO$_2$ did not form big agglomerates in any of the supports. Moreover, it can also be deduced by comparing the most intense γ-Al$_2$O$_3$ peaks {400} and {440} that these peaks become larger with the addition of ZrO$_2$, especially for the ZrAl P support.

The Co$_3$O$_4$ and Co mean particle sizes as estimated by X-ray diffraction are presented in Table 4. The H$_2$ and CO chemisorption results are presented in Table 5. As can be observed, the metal dispersion is similar but somewhat higher for the Zr-promoted catalysts. As a result, the mean Co particle size of these two catalysts is smaller than that of the CoAl. The results may be in
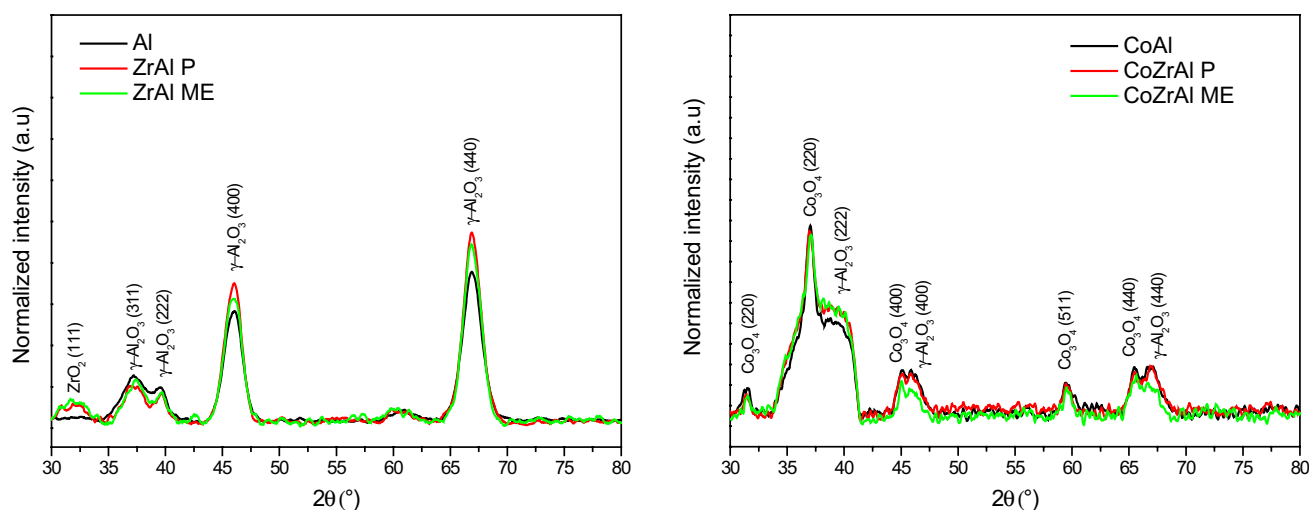
Fig. 6 X-ray diffractograms of the supports (*left*) and catalysts (*right*)

Table 5 H$_2$ and CO chemisorption results after in situ reduction at 350 °C for 16 h in H$_2$ flow

Catalyst	Total H$_2$ uptake (μmol/g)	Irreversible H$_2$ uptake (μmol/g)	D (%)[a]	d(Co^0)$_H$ (nm)[b]	Total CO uptake (μmol/g)	Irreversible CO uptake (μmol/g)	CO/Co$_s$[c]
CoAl	48	27	4.7	9	64	42	0.44
CoZrAl P	51	27	5.0	8	71	44	0.43
CoZrAl ME	58	32	5.7	7	74	47	0.41

[a]Metal dispersion as estimated using the total H$_2$ uptake and assuming a H:Co stoichiometry equal to 1:1

[b]Mean Co particle size as estimated using the DOR and the metal dispersion and assuming spherical particles

[c]Relationship between the irreversible CO uptake and the number of Co^0 active sites estimated by H$_2$ chemisorption

disagreement with the Co particle size obtained by XRD. According to the XRD results, the Zr-modified catalysts should have presented a similar mean Co particle size. The Co particle size for the CoAl catalyst is, nevertheless, in better agreement with that obtained by XRD.

A possible explanation to this discrepancy between XRD and H_2 chemisorption is that XRD is performed on calcined samples and that the calculation of the Co particle size assumes particle integrity during reduction. Another explanation could be the adsorption of H_2 on the support. Enache et al. [51] found by means of H_2 temperature-programmed desorption analyses that hydrogen can chemisorb on ZrO_2. In that case, the metal dispersion obtained for the Zr-modified catalysts would be overestimated. It may also be wrong to assume that the mean Co particle size can be estimated using the molar volumes of Co_3O_4 and Co metallic, especially if only part of the cobalt in the catalyst is present as Co_3O_4 after calcination. Finally, it cannot be discarded that the differences in Co particle size are due to other intrinsic errors of these techniques (e.g. assuming spherical particles).

In order to offer a better understanding of the chemisorption results, it was found convenient to determine the irreversible H_2 and CO uptakes. Since it is improbable that the reversibility of chemisorbed H_2 on Co is identical to that on ZrO_2, the ratio between irreversible and total uptakes should be different for these catalysts. Nevertheless, this ratio is very similar for the three samples (between 0.53 and 0.56). Therefore, H_2 probably does not chemisorb on these supports.

Furthermore, the CO uptakes are similar but also slightly larger for the Zr-promoted catalysts. The catalysts may however present different CO:Co adsorption stoichiometry due to a different metal dispersion and/or metal-support interaction. According to Reuel and Bartholomew [26], the relation between the irreversible CO uptake and the number of Co active sites estimated by H_2 chemisorption (named CO/Co_s in Table 5) is representative of the CO adsorption stoichiometry. A CO/Co_s value of ca. 0.4, which corresponds to poorly dispersed cobalt [26], was found for the three catalysts. Therefore, the presented CO uptakes may also be illustrative of the number of Co active sites.

On the basis of the information gathered, it can be concluded that the porosity, reducibility and metal dispersion of the catalysts are similar. The main difference between these catalysts remains on the presence and dispersion of ZrO_2. As a result, these three catalysts appear to be a convenient set for studying the influence of ZrO_2 on the activity and selectivity of Co/γ-Al_2O_3 FT catalysts.

3.2 Catalytic Tests

3.2.1 Activity and Stability of the Catalysts

The CO conversion as function of time on stream is presented in Fig. 7 for the three catalysts. As explained previously, the tests consisted of four periods. In Period I, the catalysts were tested at a GHSV of 10 NL/h-$g_{catalyst}$ in order to compare their activity. In Periods II, III and IV the GHSV was adjusted in order to operate at CO conversions of ca. 30, 40 and 50%, respectively. The GHSV employed in each period and the corresponding average CO conversions are presented in Table 6.

As can be deduced by comparing the CO conversions in the first period, the catalyst activity decreases in the order CoZrAl P > CoAl > CoZrAl ME. The initial activity (time on stream = 5 h) was further used for estimation of the turnover frequencies. The Site Time Yield (STY's), based on the metal dispersion estimated by H_2 chemisorption, are presented in Fig. 8. As can be seen, the STY of the catalysts also decreases in the order CoZrAl P > CoAl > CoZrAl ME; fact that could be expected since the catalysts presented similar cobalt dispersion.

As explained previously, Period IV served for comparison of the catalyst deactivation rates. The results in Period IV suggest that Zr does not have any significant influence on catalyst stability (see Fig. 7). Nevertheless, the CoAl catalyst exhibited a more stable performance than the other catalysts in Period I. The addition of ZrO_2 may therefore enhance the deactivation rate at the beginning of the reaction. This observation is in line with the work of Ma et al. [24] who also found faster deactivation rates for Zr-modified catalysts, especially in the first 24 h.
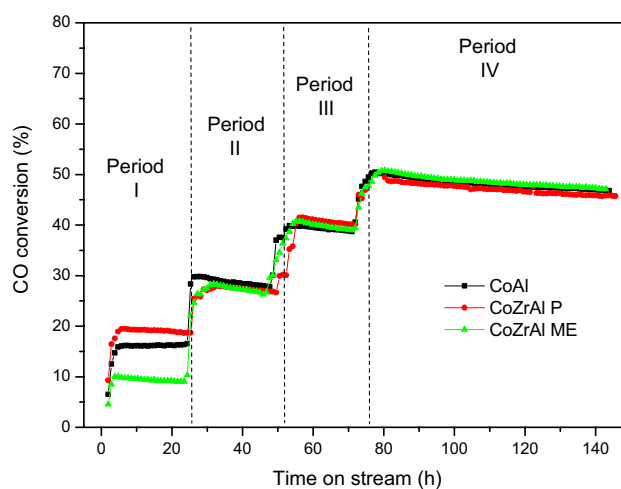

Fig. 7 CO conversion as function of time on stream. Operating conditions: 20 bar, 210 °C and H_2/CO =2.1

Table 6 Gas hourly space velocities and average CO conversion in the different periods

Catalysts	Syngas GHSV [NL/(h g$_{catalyst}$)]				Average CO conversion (%)			
	Period I	Period II	Period III	Period IV	Period I	Period II	Period III	Period IV[a]
CoAl	10	5.7	4.0	3.0	16.2	28.9	39.3	49.6
CoZrAl P	10	6.5	4.2	3.4	19.1	27.3	40.7	48.2
CoZrAl ME	10	3.3	2.0	1.4	9.4	27.4	39.8	49.9

[a]Average conversion for the first 20 h in Period IV

In conclusion, the results indicate that Zr can have either a positive or a negative effect on catalyst activity. The CoZrAl P catalyst, which presented a Zr-poor distribution, exhibited an increase in activity. Contrariwise, the CoZrAl ME catalyst, which presented a homogeneous distribution, showed a lower activity than the CoAl catalyst. Unfortunately, these results cannot be explained by differences in support acidity, factor that is believed to play a crucial role in the FTS activity [46, 47]. According to Johnson and Bell [33], promotion with Zr originates from sites with enhanced activity at the Co-ZrO$_2$ interface. The results are therefore surprising since a larger contact between ZrO$_2$ and cobalt and thus, a higher activity, was expected for the CoZrAl ME catalyst.

A possible explanation to this contradicting effect may be a faster deactivation of the Zr-modified catalysts occurring during the reaction start-up. If that was the case, the activities observed after 5 h on stream would not be representative of the actual initial activity of the catalysts. In other words, Zr may have enhanced the activity of the two catalysts but it also accelerated their initial deactivation rate, especially for the CoZrAl ME catalyst.

Recently, the existence of CO-induced Ostwald ripening has been identified as a potential cause of deactivation in cobalt FT catalysts [52, 53]. This phenomenon is favored at high CO partial pressures and low temperatures [54, 55] and so at the start-up conditions of the present study (180–210 °C and 20 bar). Moreover, Ostwald ripening, i.e.

migration of small cobalt clusters or monoatomic species from small to large crystallites, is especially detrimental in FTS. This deactivation mechanism results in the creation of large crystallites but also very small cobalt clusters, the latter being particularly inactive in FTS [56–58] and prone to re-oxidation [59–62].

Another possible explanation is simply that Zr enhances the cobalt oxidation rate. According to van Steen et al. [62], oxidation of cobalt is only thermodynamically feasible at sufficiently high conversions and for particles smaller than 4–5 nm. Nevertheless, oxidation in the form of cobalt aluminates is spontaneous under relevant FTS conditions and favored at low temperatures [63]. However it is claimed that this reaction is kinetically restricted [61]. The situation may be different, nonetheless, with Zr-promoted catalysts.

It is therefore speculated that the addition of Zr can decrease the catalyst stability under the start-up conditions. Indeed, Rohr et al. [15] found that the effect of Zr on the catalyst activity at high pressure FTS conditions was not as significant as its effect at low pressure conditions. Johnson and Bell [33] also observed that the promoting effect of Zr on Co/SiO$_2$ was already very small at syngas pressures of 10 bar and a temperature of 210 °C. This decreasing promoting effect of Zr with increasing pressure, together with a faster deactivation, may explain the low performance of the CoZrAl ME catalyst.

3.2.2 Selectivity of the Catalysts

As already mentioned, the selectivity of the catalysts was compared at CO conversions of 30, 40 and 50% in Periods II, III and IV, respectively. Figure 9 shows the selectivity to methane and long chain hydrocarbons (C5+) in the different periods. The results show that the selectivity to methane decreases with conversion while the selectivity to C5+ increases, as expected [41, 49, 64]. Furthermore, the results show that addition of Zr reduces the selectivity to methane and favors the selectivity to C5+. This effect is particularly pronounced for the CoZrAl ME catalyst. This effect is, nevertheless, only observed when comparing the CoAl and CoZrAl P in Periods III and IV. It may also be noted that the same effect is observed in Period I even though the CO conversion was the lowest for the CoZrAl ME catalyst. This higher selectivity to long chain hydrocarbons obtained
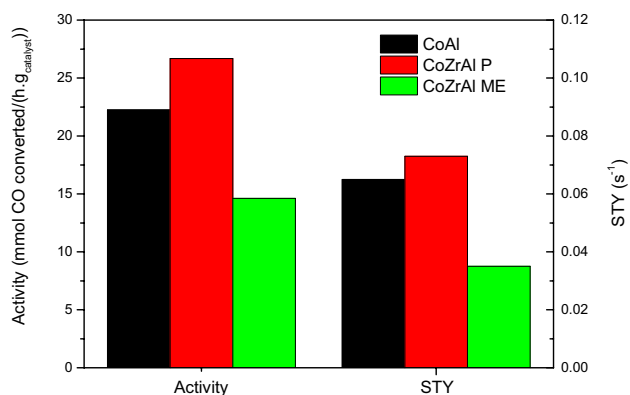
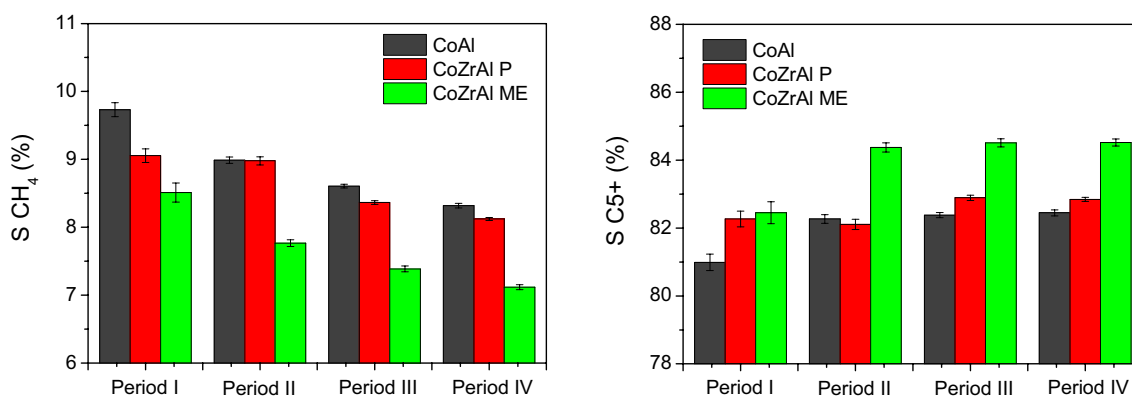**Fig. 8** Initial activity (time on stream = 5 h) and site time yield (STY) for the three catalysts

Fig. 9 Selectivity to methane (*left*) and selectivity to long chain hydrocarbons (*right*). The *error bars* represent the standard error of the mean value

for the CoZrAl ME catalyst may be ascribed to its slightly higher support acidity.

The selectivity to C2-C4 hydrocarbons and CO_2 is presented in Fig. 10. The results show that the CoZrAl ME presents a lower selectivity to these short-chain hydrocarbons. The selectivity to CO_2 was almost negligible for all the catalysts but some small differences between the CoZrAl ME catalysts and the others could be detected. Apparently, ZrO_2 can enhance either the water-gas-shift activity or favor the Boudouard reaction. The fact that the CoZrAl ME catalyst presents higher CO_2 selectivity may be ascribed to a larger concentration of CoO in the catalyst. A larger concentration of unreduced cobalt could explain its lower activity.

Figure 11 shows the olefin-to-paraffin ratio and the selectivity to branched hydrocarbons (iso-butane and iso-butene) for the three catalysts. As can be seen the olefin-to-paraffin ratio (o/p) decreases remarkably with increasing conversion. For instance, the ethylene-to-ethane ratio decreases almost by half from Period II to Period III. Moreover, the CoZrAl ME catalyst presents a significantly higher ethylene-to-ethane ratio. In general, Zr seems to increase the o/p for C3 and C4 hydrocarbons as well, particularly for the CoZrAl P catalyst. Finally, the results also showed a very low selectivity to branched C4 hydrocarbons for the three catalysts. The addition of Zr shows a slight decrease in the yield to branched products. However the differences are quite small in the latter case.

Finally, it may be interesting to mention that this significantly higher ethylene-to-ethane ratio found for the CoZrAl ME, suggests that ethylene re-adsorption and further polymerization [65] is inhibited by the presence of Zr. In consequence, the higher SC5+ observed when adding Zr, is likely to be due to an enhancement of the primary polymerization activity but not to an enhancement of secondary reactions.
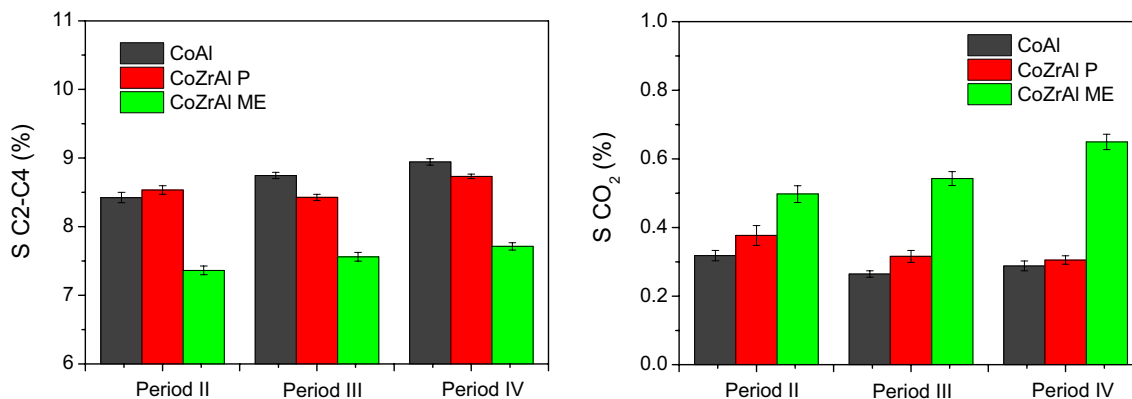

Fig. 10 Selectivity to C2-C4 hydrocarbons (*left*) and CO_2 (*right*)
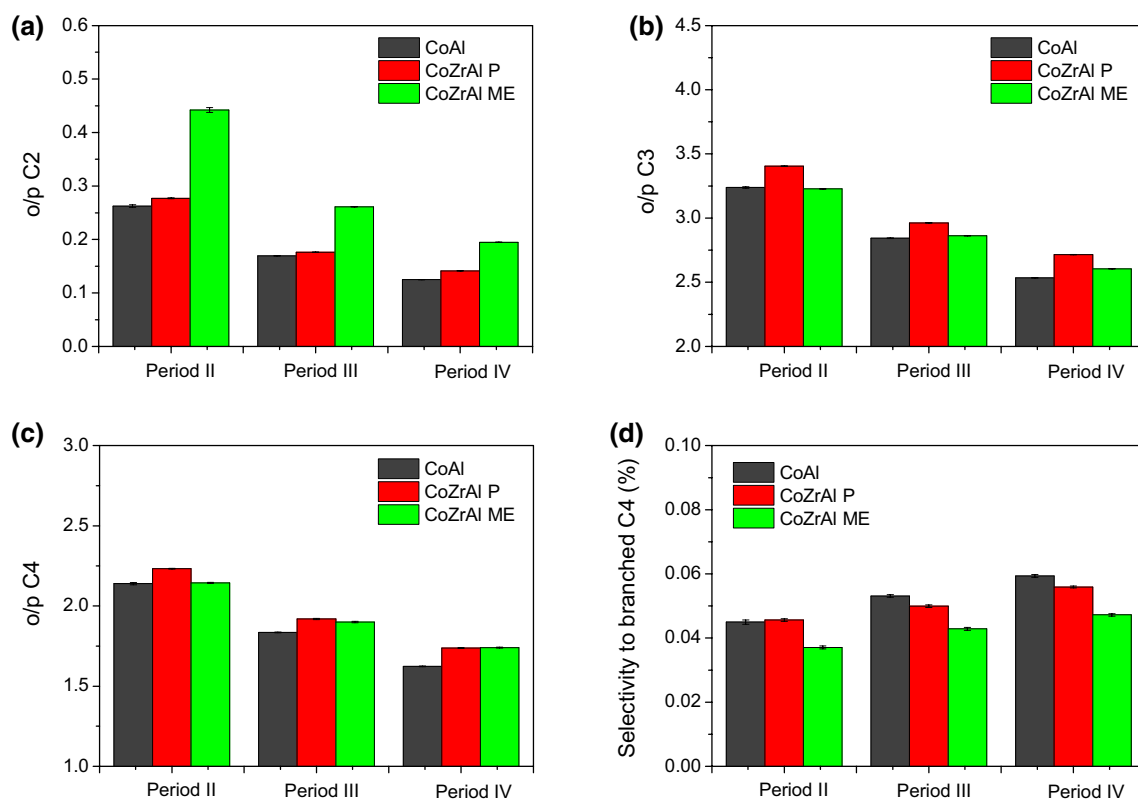
Fig. 11 Selectivity to olefins and branched hydrocarbons: **a** Olefin-to-paraffin ratio in C2 hydrocarbons. **b** Olefin-to-paraffin ratio in C3 hydrocarbons. **c** Olefin-to-paraffin ratio in C4 hydrocarbons and **d** Selectivity to branched C4 hydrocarbons

4 Conclusions

In the present work, two Zr-modified alumina supports were synthetized containing the same amount of Zr but a different distribution of this promoter over the alumina surface. These supports, together with the unmodified alumina, were used to prepare cobalt-based catalysts with similar porosity and cobalt dispersion. The three catalysts were further used to study any possible effects of Zr on the catalyst reducibility and performance in the Fischer–Tropsch synthesis.

The results indicate that neither the addition of Zr nor the distribution of this promoter enhance the catalyst reducibility. This observation may be ascribed to an uncomplete coverage of the alumina surface, insufficient to avoid the formation cobalt-aluminate species.

The FT activity was enhanced when using a carrier consisting of large ZrO_2 islands over the alumina surface. Contrariwise, the use of a carrier with a homogeneous Zr distribution led to a decrease in activity. This contradictory effect may be explained by a faster initial deactivation rate of Zr-modified catalysts, which is more pronounced when this promoter is homogeneously dispersed. This issue must be clarified prior to recommending the use of Zr as

a promoter in Co/γ-Al$_2$O$_3$ catalysts. Besides this adverse effect, the addition of Zr favored the selectivity to long chain hydrocarbons and ethylene, especially when Zr was homogeneously dispersed.

References

1. Dry ME (2002) The Fischer–Tropsch process: 1950–2000. Catal Today 71:227–241

2. Tijmensen MJA, Faaij APC, Hamelinck CN, Van Hardeveld MRM (2002) Exploration of the possibilities for production of Fischer Tropsch liquids and power via biomass gasification. Biomass Bioenergy 23:129–152

3. Iglesia E (1997) Design, synthesis, and use of cobalt-based Fischer–Tropsch synthesis catalysts. Appl Catal A 161:59–78

4. Khodakov AY, Chu W, Fongarland P (2007) Advances in the development of novel cobalt Fischer–Tropsch catalysts for synthesis of long-chain hydrocarbons and clean fuels. Chem Rev 107:1692–1744

5. Tsakoumis NE, Rønning M, Borg Ø, Rytter E, Holmen A (2010) Deactivation of cobalt based Fischer–Tropsch catalysts: a review. Catal Today 154:162–182

6. Rytter E, Holmen A (2015) Deactivation and Regeneration of Commercial Type Fischer-Tropsch Co-Catalysts - A Mini-Review. Catalysts 5:478–499

7. Schanke D, Vada S, Blekkan EA, Hilmen AM, Hoff A, Holmen A (1995) Study of Pt-promoted cobalt CO hydrogenation catalysts. J Catal 156:85–95

8. Borg Ø, Eri S, Blekkan EA, Storsæter S, Wigum H, Rytter E, Holmen A (2007) Fischer–Tropsch synthesis over γ-alumina-supported cobalt catalysts: effect of support variables. J Catal 248:89–100

9. Ma W, Jacobs G, Keogh R, Yen CH, Klettlinger JLS, Davis BH (2011) Fischer–Tropsch synthesis: effect of Pt promoter on activity, selectivities to hydrocarbons and oxygenates, and kinetic parameters over 15%Co/Al₂O₃. In: Synthetic Liquids Production and Refining, Chap 6. American Chemical Society, pp 127–153

10. Borg Ø, Hammer N, Eri S, Lindvåg OA, Myrstad R, Blekkan EA, Rønning M, Rytter E, Holmen A (2009) Fischer–Tropsch synthesis over un-promoted and Re-promoted γ-Al₂O₃ supported cobalt catalysts with different pore sizes. Catal Today 142:70–77

11. Jacobs G, Patterson PM, Zhang Y, Das T, Li J, Davis BH (2002) Fischer–Tropsch synthesis: deactivation of noble metal-promoted Co/Al2O3 catalysts. Appl Catal A 233:215–226

12. Nabaho D, Niemantsverdriet JW, Claeys M, Van Steen E (2016) Hydrogen spillover in the Fischer–Tropsch synthesis: an analysis of platinum as a promoter for cobalt-alumina catalysts. Catal Today 261:17–27

13. Jacobs G, Chaney JA, Patterson PM, Das TK, Davis BH (2004) Fischer–Tropsch synthesis: study of the promotion of Re on the reduction property of Co/Al2O3 catalysts by in situ EXAFS/XANES of Co K and Re LIII edges and XPS. Appl Catal A 264:203–212

14. Jacobs G, Chaney JA, Patterson PM, Das TK, Maillot JC, Davis BH (2004) Fischer–Tropsch synthesis: study of the promotion of Pt on the reduction property of Co/Al₂O₃ catalysts by in situ EXAFS of Co K and Pt LIII edges and XPS. J Synchrotron Radiat 11:414–422

15. Rohr F, Lindvåg OA, Holmen A, Blekkan EA (2000) Fischer–Tropsch synthesis over cobalt catalysts supported on zirconia-modified alumina. Catal Today 58:247–254

16. Jongsomjit B, Panprabot J, Goodwin JG Jr (2003) Effect of zirconia-modified alumina on the properties of Co/γ -Al₂O₃ catalysts. J Catal 215:66–77

17. Zhang J, Zhao H, Chen J, Ren J, Sun Y, Xie Y, Hu T, Liu T (2002) Influence of zirconia promoter on catalytic performance of cobalt catalysts for Fischer–Tropsch Synthesis. Chin J Catal 23:533–534

18. Ledford JS, Houalla M, Proctor A, Hercules DM, Petrakis L (1989) Influence of lanthanum on the surface structure and CO hydrogenation acitivity of supported cobalt catalysts. J Phys Chem 93:6770–6777

19. Zhang Y, Xiong H, Liew K, Li J (2005) Effect of magnesia on alumina-supported cobalt Fischer–Tropsch synthesis catalysts. J Mol Catal A 237:172–181

20. Shimura K, Miyazawa T, Hanaoka T, Hirata S (2015) Fischer–Tropsch synthesis over alumina supported cobalt catalyst: effect of promoter addition. Appl Catal A 494:1–11

21. Park SJ, Kim SM, Woo MH, Bae JW, Jun KW, Ha KS (2012) Effects of titanium impurity on alumina surface for the activity of Co/Ti-Al₂O₃ Fischer–Tropsch catalyst. Appl Catal A 419–420:148–155

22. Dai X, Yu C, Shen S (2001) Promotion effect of ceria on fischer-tropsch synthesis performance over Co/Al₂O₃ catalyst. Chin J Catal 22:104–108

23. Jacobs G, Das TK, Zhang Y, Li J, Racoillet G, Davis BH (2002) Fischer–Tropsch synthesis: support, loading, and promoter effects on the reducibility of cobalt catalysts. Appl Catal A 233:263–281

24. Ma W, Jacobs G, Gao P, Jermwongratanachai T, Shafer WD, Pendyala VRR, Yen CH, Klettlinger JLS, Davis BH (2014) Fischer–Tropsch synthesis: pore size and Zr promotional effects on the activity and selectivity of 25% Co/Al₂O₃ catalysts. Appl Catal A 475:314–324

25. Xiong H, Zhang Y, Liew K, Li J (2005) Catalytic performance of zirconium-modified Co/Al₂O₃ for Fischer–Tropsch synthesis. J Mol Catal A 231:145–151

26. Reuel RC, Bartholomew CH (1984) The stoichiometries of H₂ and CO adsorptions on cobalt: effects of support and preparation. J Catal 85:63–77

27. Mu S, Li D, Hou B, Jia L, Chen J, Sun Y (2010) Influence of ZrO₂ loading on SBA-15-supported cobalt catalysts for Fischer–Tropsch synthesis. Energy Fuels 24:3715–3718

28. Feller A, Claeys M, van Steen E (1999) Cobalt cluster effects in zirconium promoted Co/SiO₂ Fischer–Tropsch catalysts. J Catal 185:120–130

29. Oukaci R, Singleton AH, Goodwin JG Jr (1999) Comparison of patented Co F-T catalysts using fixed-bed and slurry bubble column reactors. Appl Catal A 186:129–144

30. Moradi GR, Basir MM, Taeb A, Kiennemann A (2003) Promotion of Co/SiO₂ Fischer–Tropsch catalysts with zirconium. Catal Commun 4:27–32

31. Ali S, Chen B, Goodwin JG (1995) Zr promotion of Co/SiO₂ for Fischer–Tropsch synthesis. J Catal 157:35–41

32. Hong J, Chu W, Chernavskii PA, Khodakov AY (2010) Effects of zirconia promotion on the structure and performance of smaller and larger pore silica-supported cobalt catalysts for Fischer–Tropsch synthesis. Appl Catal A 382:28–35

33. Johnson GR, Bell AT (2016) Role of ZrO₂ in promoting the activity and selectivity of co-based Fischer–Tropsch synthesis catalysts. ACS Catal 6:100–114

34. Eriksson S, Nylén U, Rojas S, Boutonnet M (2004) Preparation of catalysts from microemulsions and their applications in heterogeneous catalysis. Appl Catal A 265:207–219

35. Emeis CA (1993) Determination of integrated molar extinction coefficients for infrared absorption bands of pyridine adsorbed on solid acid catalysts. J Catal 141:347–354

36. Bartholomew CH, Farrauto RJ (2010) Fundamentals of industrial catalytic processes, 2nd edn. Wiley, Hoboken

37. Lemaitre JL, Delannay F (1984) Characterization of heteogeneous catalysts. Marcel Dekker, New York

38. Lögdberg S, Lualdi M, Järås S, Walmsley JC, Blekkan EA, Rytter E, Holmen A (2010) On the selectivity of cobalt-based Fischer–Tropsch catalysts: evidence for a common precursor for methane and long-chain hydrocarbons. J Catal 274:84–98

39. Rytter E, Schanke D, Eri S, Wigum H, Skagseth TH, Sinkadu N (2004) Optimization of statoil's Fischer-Tropsch Co/Re/alumina catalyst. Preprints- American Chemical Society Division Of Petroleum Chemistry, Washington, DC

40. Lualdi M, Lögdberg S, Di Carlo G, Järås S, Boutonnet M, Venezia AM, Blekkan EA, Holmen A (2011) Evidence for

diffusion-controlled hydrocarbon selectivities in the Fischer–Tropsch synthesis over cobalt supported on ordered mesoporous silica. Top Catal 54:1175–1184

41. Borg O, Yu Z, Chen D, Blekkan EA, Rytter E, Holmen A (2014) The effect of water on the activity and selectivity for carbon nanofiber supported cobalt Fischer–tropsch catalysts. Top Catal 57:491–499

42. Lualdi M, Lögdberg S, Boutonnet M, Järås S (2013) On the effect of water on the Fischer–Tropsch rate over a Co-based catalyst: the influence of the H_2/CO ratio. Catal Today 214:25–29

43. Lualdi M, Lögdberg S, Regali F, Boutonnet M, Järås S (2011) Investigation of mixtures of a Co-based catalyst and a Cu-based catalyst for the Fischer–tropsch synthesis with bio-syngas: the importance of indigenous water. Top Catal 54:977–985

44. Santos PS, Santos HS, Toledo SP (2000) Standard transition aluminas. Electron microscopy studies. Mater Res 3:104–114

45. Rozita Y, Brydson R, Comyn TP, Scott AJ, Hammond C, Brown A, Chauruka S, Hassanpour A, Young NP, Kirkland AI, Sawada H, Smith RI (2013) A Study of commercial nanoparticulate γ-Al_2O_3 catalyst supports. ChemCatChem 5:2695–2706

46. Prieto G, De Mello MIS, Concepción P, Murciano R, Pergher SBC, Martínez A (2015) Cobalt-Catalyzed Fischer–Tropsch Synthesis: Chemical Nature of the Oxide Support as a Performance Descriptor. ACS Catal 5:3323–3335

47. Johnson GR, Bell AT (2016) Effects of Lewis acidity of metal oxide promoters on the activity and selectivity of Co-based Fischer–Tropsch synthesis catalysts. J Catal 338:250–264

48. Jermwongratanachai T, Jacobs G, Ma W, Shafer WD, Gnanamani MK, Gao P, Kitiyanan B, Davis BH, Klettlinger JLS, Yen CH, Cronauer DC, Kropf AJ, Marshall CL (2013) Fischer–Tropsch synthesis: comparisons between Pt and Ag promoted Co/Al_2O_3 catalysts for reducibility, local atomic structure, catalytic activity, and oxidation-reduction (OR) cycles. Appl Catal A 464–465:165–180

49. Hilmen AM, Schanke D, Hanssen KF, Holmen A (1999) Study of the effect of water on alumina supported cobalt Fischer–Tropsch catalysts. Appl Catal A 186:169–188

50. Barrientos J, Montes V, Boutonnet M, Järås S (2016) Further insights into the effect of sulfur on the activity and selectivity of cobalt-based Fischer–Tropsch catalysts. Catal Today 275:119–126

51. Enache DI, Roy-Auberger M, Revel R (2004) Differences in the characteristics and catalytic properties of cobalt-based Fischer–Tropsch catalysts supported on zirconia and alumina. Appl Catal A 268:51–60

52. Claeys M, Dry ME, van Steen E, van Berge PJ, Booyens S, Crous R, van Helden P, Labuschagne J, Moodley DJ, Saib AM (2015) Impact of process conditions on the sintering behavior of an alumina-supported cobalt Fischer–Tropsch catalyst studied with an in situ magnetometer. ACS Catal 5:841–852

53. Kistamurthy D, Saib AM, Moodley DJ, Niemantsverdriet JW, Weststrate CJ (2015) Ostwald ripening on a planar Co/SiO_2 catalyst exposed to model Fischer–Tropsch synthesis conditions. J Catal 328:123–129

54. Blanchard AA (1937) The volatile metal carbonyls. Chem Rev 21:3–38

55. Shen WM, Dumesic JA, Hill CG Jr (1981) Criteria for stable Ni particle size under methanation reaction conditions: nickel transport and particle size growth via nickel carbonyl. J Catal 68:152–165

56. Bezemer GL, Bitter JH, Kuipers HPCE, Oosterbeek H, Holewijn JE, Xu X, Kapteijn F, Van Dillen AJ, de Jong KP (2006) Cobalt particle size effects in the Fischer–Tropsch reaction studied with carbon nanofiber supported catalysts. J Am Chem Soc 128:3956–3964

57. den Breejen JP, Radstake PB, Bezemer GL, Bitter JH, Frøseth V, Holmen A, de Jong KP (2009) On the origin of the cobalt particle size effects in Fischer–Tropsch catalysis. J Am Chem Soc 131:7197–7203

58. Prieto G, Martínez A, Concepción P, Moreno-Tost R (2009) Cobalt particle size effects in Fischer–Tropsch synthesis: structural and in situ spectroscopic characterisation on reverse micelle-synthesised Co/ITQ-2 model catalysts. J Catal 266:129–144

59. Hilmen AM, Schanke D, Holmen A (1997) In: Misono M (ed) Reoxidation of supported cobalt Fischer–Tropsch catalysts. Studies in surface science and catalysis, Amsterdam

60. Schanke D, Hilmen AM, Bergene E, Kinnari K, Rytter E, Ådnanes E, Holmen A (1996) Reoxidation and deactivation of supported cobalt Fischer–Tropsch catalysts. Energy and Fuels 10:x-872

61. van de Loosdrecht J, Balzhinimaev B, Dalmon JA, Niemantsverdriet JW, Tsybulya SV, Saib AM, van Berge PJ, Visagie JL (2007) Cobalt Fischer–Tropsch synthesis: deactivation by oxidation? Catal Today 123:293–302

62. van Steen E, Claeys M, Dry ME, van de Loosdrecht J, Viljoen EL, Visagie JL (2005) Stability of nanocrystals: Thermodynamic analysis of oxidation and re-reduction of cobalt in water/hydrogen mixtures. J Phys Chem B 109:3575–3577

63. Hou C, Xia G, Sun X, Wu Y, Jin C, Yan Z, Li M, Hu Z, Nie H, Li D (2016) Thermodynamics of oxidation of an alumina-supported cobalt catalyst by water in F-T synthesis. Catal Today 264:91–97

64. Dalai AK, Davis BH (2008) Fischer–Tropsch synthesis: a review of water effects on the performances of unsupported and supported Co catalysts. Appl Catal A 348:1–15

65. Iglesia E, Reyes SC, Madon RJ (1991) Transport-enhanced α-olefin readsorption pathways in Ru-catalyzed hydrocarbon synthesis. J Catal 129:238–256